Powder Technology 420 (2023) 118418

Contents lists available at ScienceDirect

Powder Technology

journal homepage: www.journals.elsevier.com/powder-technology

Electrical capacitance tomography-based estimation of slug flow parameters in horizontally aligned pneumatic conveyors

Thomas Suppan [a,*], Markus Neumayer [a], Thomas Bretterklieber [a], Stefan Puttinger [b], Christoph Feilmayr [c], Stefan Schuster [c], Hannes Wegleiter [a]

[a] Christian Doppler Laboratory for Measurement Systems for Harsh Operating Conditions, Institute of Electrical Measurement and Sensor Systems, Graz University of Technology, Inffeldgasse 23, Graz, 8010, Austria
[b] Department of Particulate Flow Modelling, Johannes Kepler University Linz, Altenbergerstrasse 69, Linz, 4040, Austria
[c] voestalpine Stahl GmbH, voestalpine-Straße 3, Linz, 4020, Austria

HIGHLIGHTS

- Electrical capacitance tomography-based slug flow parameter estimation.
- Tomographic imaging of mass concentration distributions.
- Differentiation between slug velocity and particle velocity.
- Application within an industrial-scale pneumatic conveyor with a length of 2 km.
- Novel insights into dense phase conveying of Geldart group A powders with $Ar \approx 1e0$.

GRAPHICAL ABSTRACT

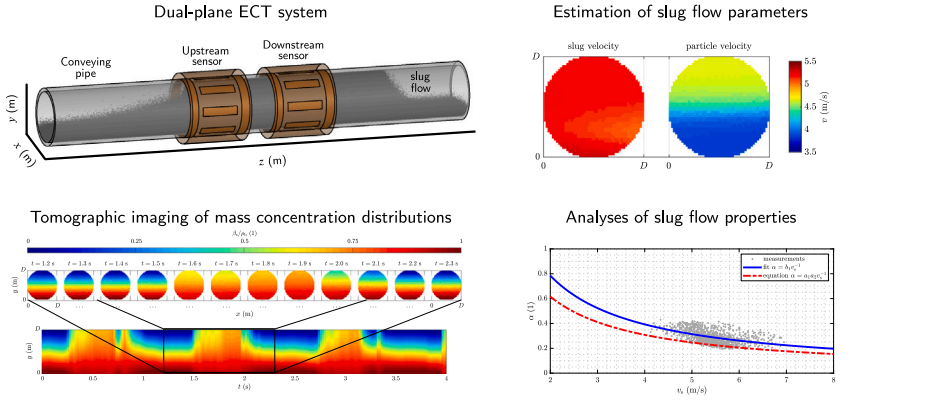

ARTICLE INFO

Keywords:
Dense phase pneumatic conveying
Horizontal slug flow
Electrical capacitance tomography
Flow parameter estimation

ABSTRACT

Pneumatic conveying is a widely applied technique for the transportation of powders. Dense phase conveying such as slug flow is the preferable operating condition of such transport systems. Advantages are the reduced energy and conveying gas consumption and reduced material wear. The design and the operation of dense phase conveyors is a challenging task due to complex flow dynamics and the lack of reliable flow meters, which are crucial for process control. In this work the capabilities of electrical capacitance tomography (ECT) for slug flow parameter estimation are analysed. The estimation of flow parameters is addressed and demonstrated by means of laboratory experiments. Amongst other parameters it is shown that mass concentration distributions as well as particle velocity fields can be obtained from tomographic image reconstruction results, which are substantial parameters for potential mass flow metering. Additionally, the proposed estimation techniques are applied to signals provided by an ECT system, which is installed within a large-scale pneumatic conveyor of an industrial process plant. It is observed that also Geldart group A powders with Archimedes numbers in the scale of $Ar \approx 1e0$ are conveyable in slug-like structures which can be separated by stationary or non-stationary layers. Furthermore, various slug flow properties of powders with $Ar > 1e2$ reported in literature are confirmed

* Corresponding author.
E-mail addresses: suppan@tugraz.at (T. Suppan), neumayer@tugraz.at (M. Neumayer), thomas.bretterklieber@tugraz.at (T. Bretterklieber), stefan.puttinger@jku.at (S. Puttinger), Christoph.Feilmayr@voestalpine.com (C. Feilmayr), Stefan.Schuster2@voestalpine.com (S. Schuster), wegleiter@tugraz.at (H. Wegleiter).

https://doi.org/10.1016/j.powtec.2023.118418
Received 2 November 2022; Received in revised form 26 January 2023; Accepted 3 March 2023
Available online 7 March 2023

but also deviating properties are observed, leading to novel insights into horizontal dense phase flow processes of powders with $Ar \approx 1e0$. The results demonstrated in this work are pointing out the capabilities of ECT for flow analyses, which are enabling further insights into flow mechanisms and future developments of flow meters for dense phase flow processes.

1. Introduction

Pneumatic conveying is a common technique for the transportation of powders where pressurized gas is utilized to carry materials through enclosed pipelines. Pneumatic conveyors can be found in a variety of industrial fields reaching from steel making and power generation to agricultural as well as pharmaceutical industries [1,2].

The resulting flow regime within a pneumatic conveyor depends on various parameters such as operating conditions, material properties as well as on geometrical properties of the pipeline. A comprehensive classification about flow regimes in horizontally aligned pneumatic conveyors can be found in [3]. A broad generalization of flow regimes can be made by differentiating between dilute flows and dense phase conveying. Dilute flow pneumatic conveying is characterized by low mass concentrations of the conveyed powder and high particle velocities. Dense phase conveying in contrast exhibit distinct phases with high particle concentrations, which are moving at lower velocities. Dense phase flows are desirable for many applications due to the reduced energy and carrier gas demand and reduced material wear compared to dilute flows [4]. The advantages of dense phase flows however come at the cost of much higher complexity with respect to the interdependencies between flow parameters and operating conditions of the conveying process. Due to the limited understanding about the complex flow dynamics the prediction of the behaviour of dense phase flows is still a major challenge making such systems difficult to design and operate reliably. The difficulty of operating dense phase conveyors stems also from the lack of reliable flow meters, which are crucial for process control.

Slug flow is a subtype of dense phase flows where the particles are moving in a wave-like motion. In horizontally aligned conveying systems these slugs are separated by stationary layers, which refers to material deposits at the bottom of the pipe. Hence, horizontal slug flow pneumatic conveying is a highly dynamical flow regime with rapidly changing spatial and temporal flow parameters. In recent years, many researchers have made great efforts to study the complex dynamics and interdependencies of flow parameters of the slug flow regime based on theoretical consideration [5–7], extensive flow experiments [8–11] as well as on simulation studies [7,12–14]. However, the analysis of dependencies between operating conditions and slug flow properties are still an important research field. Especially for large-scale conveying processes of multiple slugs, further progress is needed to understand the governing conveying mechanisms [15].

Tomographic measurement principles are promising techniques to obtain further insights in conveying processes and to advance the research in the field of dense-phase pneumatic conveying. Tomographic imaging allows visualizations of the material flow within the pipe, from which flow parameters can be derived. Amongst various process tomography techniques is electrical capacitance tomography (ECT), which has been successfully applied for flow monitoring and flow parameter estimation [16–19]. ECT utilizes capacitive measurements from an electrode array to obtain information about the material distribution within the sensor [20–22]. Fig. 1(a) illustrates a dual-plane ECT sensor used to monitor a horizontal slug flow conveying process. An ECT sensor provides cross-sectional estimates of the material distribution within the conveying pipe as it is depicted in Fig. 1(b). Dielectric characterizations of the transport good allow the estimation of mass concentration distributions from these tomographic imaging results [23,24]. Measurements of a dual-plane ECT system [17,18,25] or an electrical capacitance volume tomography (ECVT) sensor [26–28] can be utilized to obtain flow velocities and give also access to slug dimensions in axial direction as it is depicted in Fig. 1(c). Thus, ECT has the potential to provide spatial and temporal information about the material movement within the conveying process making it a practical tool for flow analyses.

In this work the capabilities of dual-plane ECT for the estimation of slug flow parameters within horizontally aligned slug flow processes are analysed. The estimation of slug flow parameters based on tomographic signal evaluations is presented. The proposed estimation techniques are demonstrated by means of slug flow experiments on a laboratory test rig, where reference data based on particle image velocimetry (PIV) [29] and visual observations is available. Hereby, a strong focus lies on parameters, which are required for the evaluation of mass flow rates, i.e. the mass concentration distribution of the transport good and the particle velocity field within the slugs. Also the estimation of other parameters is addressed, which are required for the study of slug flow processes.

Most work about ECT-based flow parameter estimation [19,30,31] as well as research on slug flow processes [8,9,32] is often limited to Geldart group B and D powders. This is mostly due to the handling of fine powers within the lab, i.e. dust generation and pollution of equipment. Although literature about dense flow pneumatic conveying of Geldart group A powders is available [33–36] the research is either limited to experiments in vertical pipelines or focuses on analysis of prevailing flow regimes. To obtain further insights into horizontal dense flow processes of Geldart group A powders the proposed estimation techniques are also applied to measurement data provided by an ECT system, which is installed within an large scale conveying process of an industrial process plant. The main contributions of this work are the demonstration of the potential of ECT for flow parameter estimation in highly dynamical slug flow processes and the analysis of the capability of ECT for potential mass flow measurements. The observations obtained from the large scale conveyor of the industrial process plant are reported and compared to slug flow properties reported in literature where consistencies and deviations are discussed in detail. Hereby, novel insights into large scale dense phase flow processes of Geldart group A powders with Archimedes numbers in the scale of $Ar \approx 1e0$ are reported. The results are pointing out the capability of ECT as a tool to analyse dense phase flows enabling further insight into complex flow mechanisms.

This paper is structured as follows. In Section 2 the experimental setup is discussed. Section 3 addresses the estimation of various slug flow parameters. In Section 4 ECT-based observations within the large scale conveyor of the industrial process plant are discussed.

2. Experimental setup

In this section the experimental setup is presented. The ECT measurement system, the laboratory flow test rig as well as the industrial field system are discussed.

2.1. ECT sensor

Both, the lab as well as the field system use a dual-plane ECT sensor with eight electrodes each. The structure of the sensor assembly is schematically depicted in Fig. 1(a). The electrodes are equidistantly

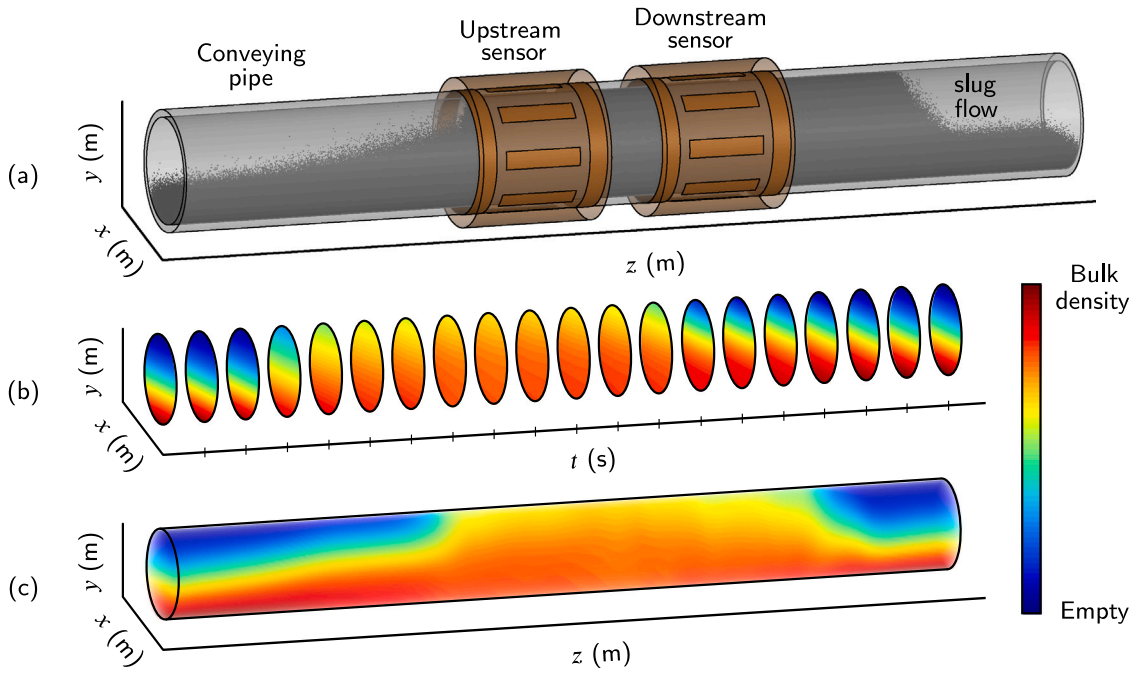

Fig. 1. (a) Illustration of a dual-plane ECT system within a horizontal slug flow conveying process. (b) Time evolution of the cross-sectional material distribution. (c) Three dimensional reconstruction of a slug.

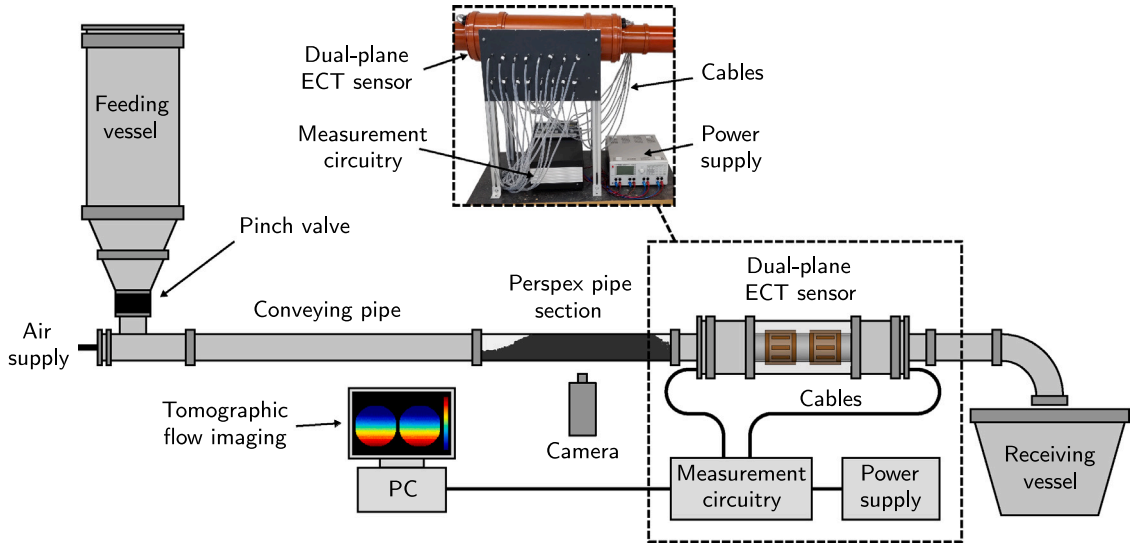

Fig. 2. Scheme of the laboratory flow test rig and a photo of the ECT measurement system.

arranged at the outer circumference of a non-conductive pipe section. In addition, both electrode planes are surrounded by a grounded shield and grounded guard rings are placed next to the electrode arrays to reduce external influences. For the lab sensor the electrode arrays are mounted on a PVC pipe as it is also used in [30].

The field sensor is assembled on a fibre composite pipe and uses an additional silicone elastomer grouting between the electrodes and the shield. The whole sensor assembly is encased in an steel pipe in order to withstand the environmental conditions within the industrial process such as high temperatures and pressures. Further information about the structure of the field sensor can be found in [37].

2.2. Measurement circuitry

In ECT all inter electrode capacitances are measured. For this purpose a displacement current-based measurement system is used, which applies an AC voltage to one electrode while the currents at the remaining electrodes are acquired [38–40]. This procedure is repeated for each electrode to measure all capacitances. In the case of a sensor with $N_{\mathrm{elec}} = 8$ electrodes, the number of measurements is given by $M = N_{\mathrm{elec}}(N_{\mathrm{elec}} - 1) = 56$. Equivalent measurement circuitries are used in the lab as well as in the field application. The dual-plane measurement system acquires data with a sampling frequency of 50 Hz in an interleaved measurement mode to avoid a crosstalk between the sensor planes. The signal to noise ratio (SNR) of the measurement system is in the range of 70 dB as it is demonstrated in [30,37].

2.3. Laboratory test rig

Fig. 2 depicts the scheme of the laboratory flow test rig, which consists of a feeding vessel, a horizontal conveying pipe and a receiving vessel. A pinch valve is used to regulate the material outflow from

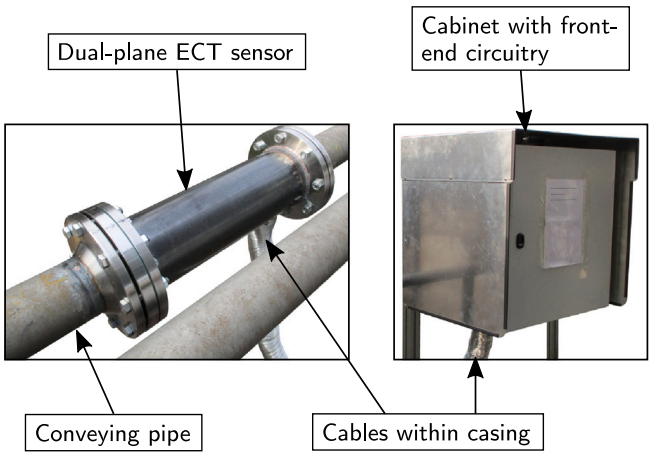

Fig. 3. Dual-plane ECT system within an large scale pneumatic conveyor of an industrial process plant.

the feeding vessel to the conveying pipe and pressurized air is used to convey the materials. A section of the conveying pipe is made of perspex for visual observations and PIV analyses of the material flow. For this purpose a camera with a frame rate of 240 frames per second is used. The inner diameter of the pipe is $D = 119\,\mathrm{mm}$ and the length of the horizontal pipe is $l = 5\,\mathrm{m}$. The dual-plane ECT system is installed 3 m after the feeding vessel. Fig. 2 also shows a photo of the laboratory measurement system. The measurement system consists of the ECT sensor, the measurement circuitry, the power supply as well as a PC for data processing. For the flow experiments polypropylene (PP) pellets of prolate spheroid shape [11] are used with an density of $\rho = 905\,\mathrm{kg\,m^{-3}}$ and an average particle size of $d_{50} = 3\,\mathrm{mm}$. The material belongs to Geldart group D [41] and has an Archimedes number in the scale of $Ar \approx 1e6$, which is well suited for slug flow experiments [3]. The Archimedes number is calculated by

$$Ar = \frac{g\rho_g\left(\rho_p - \rho_g\right)d^3}{\mu^2}, \tag{1}$$

where ρ_p and ρ_g are the density of the particles and the conveying gas, respectively, g is the acceleration due to gravity, d is the diameter of the particles and μ is the dynamic viscosity of the conveying gas.

2.4. Field system

Fig. 3 depicts the ECT system installed within an industrial process plant. The pneumatic conveyor is part of a pulverized coal injection (PCI) system within a steel plant. The transported bulk material is coal powder with an average particle size of approximately $d_{50} \approx 30\,\mu\mathrm{m}$, the material belongs to Geldart group A. The conveying gas is nitrogen N_2 and the resulting Archimedes number is in the scale of $Ar \approx 1e0$ [3]. The material is pre-dried to relative humidity levels in the range of $\phi = 0.5\,\%$ to $1.5\,\%$. The pneumatic conveyor has a total length of approximately 2000 m with an inner diameter of $D = 110\,\mathrm{mm}$. The conveying pipe is made of steel and is electrically grounded. An electrical characterization [23,24] of the transport good yielded an electrical conductivity in the scale of $\sigma \approx 1\times10^{-4}\,\mathrm{S\,m^{-1}}$. Due to the conductivity of the material and the grounded and conductive pipe, triboelectric charging of the particles and the pipe wall and associated influences on the flow process as well as on the measurement process due to resulting electrostatic effects can be ruled out [42].

The ECT sensor is encased in a steel pipe due to mechanical reasons. The measurement circuitry, power supply and a PC for data processing are placed within a cabinet. The cables connecting the sensor and the measurement circuitry are also placed within a casing to protect them from mechanical damage within the process plant. The measurement system is located approximately 200 m after the feeding vessel of the pneumatic conveyor.

2.5. Tomographic image reconstruction

The reconstruction of the cross-sectional distribution of the relative permittivity $\varepsilon_r(x,y)$ by means of ECT poses an ill-posed inverse problem, which requires prior information to obtain stable estimates. For this purpose a linearized maximum a posteriori estimator (MAP) is used. The MAP estimator is specifically adapted for imaging flow patterns in horizontal pneumatic conveying processes. Detailed information about this estimation algorithm and the design of prior information can be found in [30,43–45]. In addition, the model-based temperature compensation approach presented in [37] is applied for image reconstruction within the industrial process plant due to varying process temperatures. The reconstructed cross-sectional material distributions are represented by means of pixel values on a discrete grid (i.e. finite element discretizations) whereby the pixel values are proportional to the relative permittivity of the material within the sensor.

2.6. Dielectric characterization of fluidized powders for mass concentration estimation

In ECT different materials within the sensor are distinguished by their dielectric properties i.e. the relative permittivity ε_r [20,21]. For this reason the tomographic imaging results obtained by ECT are given by cross-sectional permittivity distributions $\varepsilon_r(x,y)$ within the sensor. For the analysis of flow process and for the estimation of flow parameters however, the estimation of mass concentration distributions of the conveyed powder is required. The mass concentration is defined as the mass m of the particles over the total volume V_{pow} of the powder $\beta = m/V_{pow}$ in $\mathrm{kg\,m^{-3}}$.

The relationship between the relative permittivity ε_r and the mass concentration β of a fluidized powder is known to follow a non-linear relationship. Recently the authors proposed a measurement methodology to characterize the dielectric properties of fluidized powders as a function of its mass concentration. The measurement principle is based on impedance measurements of a coaxial probe and weighting of the solid content within the defined volume of the coaxial probe [23]. Fig. 4 depicts the measurement setup to characterize the dielectric material properties of fluidized powders. The setup consists of a coaxial probe which allows the fluidization of the probe filling by means of an air supply [24], a network analyser to acquire the probe impedance and a balance for the weighting of the probe filling.

A suitable model to describe the relationship between the relative permittivity and the mass concentration of a fluidized powder is the Landau–Lifshitz–Looyenga (LLL) equation [23]. The LLL equation states a linear relationship between the cubic root of the relative permittivity and the mass concentration $\sqrt[3]{\varepsilon_r} = \lambda\beta + 1$ [46,47]. The measurement methodology presented in [23] is used to identify the model parameter λ for a specific material. Applying the LLL equation to the pixel values of a reconstructed permittivity distribution $\varepsilon_r(x,y)$ yields the mass concentration distribution $\beta(x,y)$ of a powder within the sensor [30, 48]. With this the ECT-based estimation of further flow parameters is enabled.

3. Estimation of slug flow parameters

In this section the estimation of slug flow parameters from tomographic signal evaluations is discussed. The focus lies on slug flow parameters, which are crucial for the understanding of the underlying flow mechanisms [9,49], for pressure drop prediction [32] as well for a potential mass flow measurement in such dense phase conveying processes.

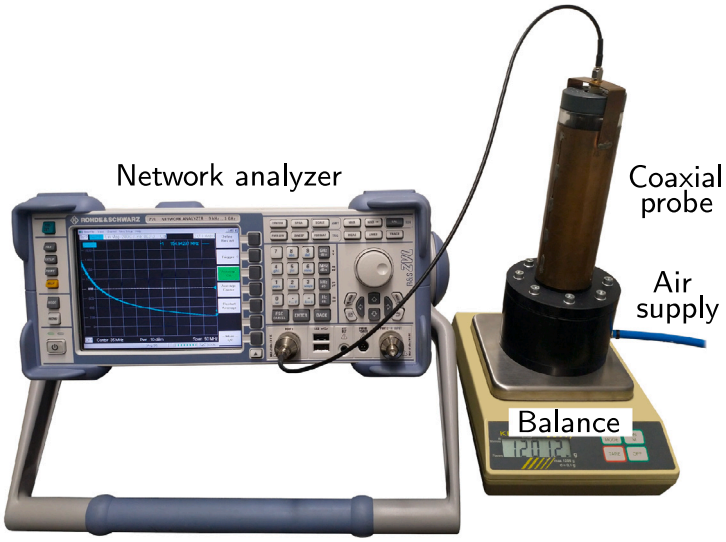

Fig. 4. Measurement setup for the dielectric characterization of fluidized powders [23,24].

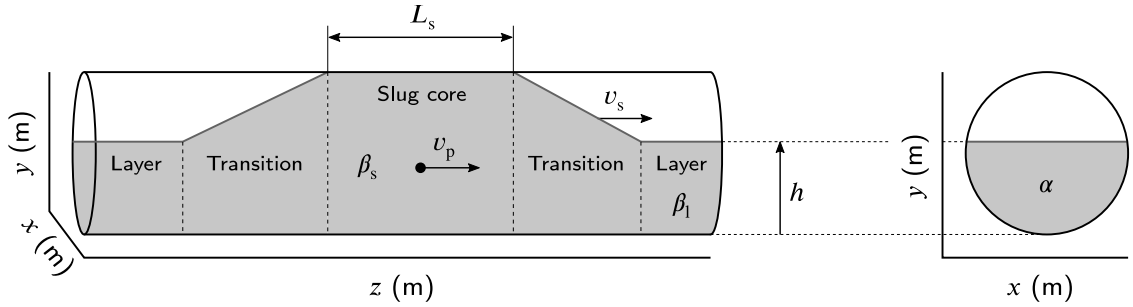

Fig. 5. Sketch of a slug showing important slug flow parameters [9,50].

3.1. Definition of slug parameters

Fig. 5 depicts a sketch of a slug showing several slug parameters which are of importance. The slug concentration β_s in $\mathrm{kg\,m^{-3}}$ is defined as the average mass concentration of the slug core, which refers to the part of the slug where the whole cross-section of the pipe is filled with material. The layer concentration β_l in $\mathrm{kg\,m^{-3}}$ refers to the concentration of the layer between consecutive slugs, which is in the case of stationary layers equal to the bulk density ρ_b of the conveyed powder, i.e. $\beta_l = \rho_b$ [9,11]. The dimensionless layer fraction α is defined as the area occupied by the layer relative to the total cross-sectional area of the conveying pipe and h denotes the height of the layer in m. The slug length L_s is defined as the length of the slug core in m. In horizontal slug flow processes with stationary layers the slug is constantly picking up material from the layer ahead of the slug and depositing material at the rear of the slug, which forms the new stationary layer. Hence, there is a relative motion between the slug and the particles, which are travelling within the slug. For this reason, a distinction must be made between the slug velocity v_s in $\mathrm{m\,s^{-1}}$ and particle velocity v_p in $\mathrm{m\,s^{-1}}$ since in general $v_s > v_p$ holds [9,32,50].

3.2. Slug concentration and layer concentration

Fig. 6 depicts the estimated mass concentration distribution of a slug, which was generated on the flow test rig in the laboratory with PP pellets. The upper plot shows the cross-sectional mass concentration distribution $\beta(x, y)$ for certain time steps. Hereby D denotes the diameter of the pipe. From this representation the stationary layers at the slug front and rear can be seen at $t = 0\,\mathrm{s}$ and $t = 2.5\,\mathrm{s}$, respectively. The transition between the layer and the slug is shown at $t = 0.5\,\mathrm{s}$ and the time steps $t = 1\,\mathrm{s}$ to $t = 2\,\mathrm{s}$ depict the slug core. Since the reconstructed material distribution was observed to be approximately constant along the horizontal x-axis the lower representation shows the height profile of the mass concentration over time $\beta(y, t)$, which allows a more compact representation of the slug compared to a sequence of cross-sectional images. Note that the colour scale shows the mass concentration normalized by the bulk density ρ_b of the material. Hence, a value of one corresponds to ρ_b. The reconstructed stationary layers show a mass concentration equal to the bulk density at the bottom of the pipe [9]. However, the boundary between the layer and the empty part of the pipe is blurred. This is due to the soft field nature of ECT, which prevents the reconstruction of sharp boundaries [21]. Yet, the stationary layer can be clearly identified. The transition zones show the filling of the pipe with the transport good and a loosening of the material bed from the layer due to the approaching slug [11]. At the front of the slug core the material shows a lower mass concentration in the upper part of the pipe [32,51]. The remaining part of the slug core shows a constant mass concentration distribution, which is lower than the material in the stationary layer. This corresponds to the results reported in [11]. The good fit between the demonstrated ECT-based mass concentration estimation and observations reported in literature confirms the applicability of ECT for estimating mass concentration distributions in slug flow processes [9,11,32,51].

For the analysis of flow mechanisms in horizontal slug flow processes parameters such as the slug concentration β_s, the layer concentration β_l, or the concentration ratio $E = \beta_s/\beta_l$ are of particular interest [9,11,32,49].

From the estimated mass concentration distribution the layer concentration β_l can be determined from the material value at the bottom

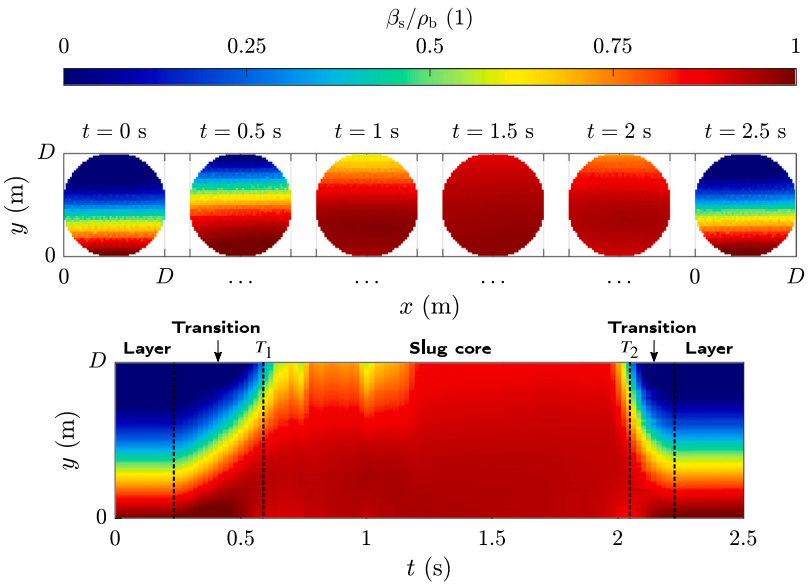

Fig. 6. Estimated mass concentration distribution of a slug flow experiment on the laboratory test rig with a Geldart group D powder with $Ar \approx 1e6$.

of the pipe, i.e. $\beta_l = \beta(y = 0)$. The slug concentration β_s can be determined from the ECT reconstruction by computing the average value of the mass concentration distribution over the slug core by

$$\beta_s = \frac{1}{T_s \Gamma} \int_{t=T_1}^{T_2} \iint_{\Gamma} \beta(x, y, t)\, \mathrm{d}x\, \mathrm{d}y\, \mathrm{d}t, \tag{2}$$

where $\Gamma = (D/2)^2 \pi$ denotes the cross section of the pipe. $T_s = T_2 - T_1$ is the duration of the slug core and T_1 and T_2 are the beginning and the end of the slug core time segment, respectively.

3.3. Layer fraction and layer height

The layer fraction α is defined by the fraction of the cross section of the conveying pipe, which is occupied by the stationary layer. α can be determined from the cross-sectional average mass concentration β of the ECT reconstruction of a stationary layer, e.g. the time step $t = 0$ s depicted in Fig. 6. β is computed by integrating the mass concentration distribution $\beta(x, y)$ over the cross-section Γ of the pipe. In [30] it is shown, that the integral over the mass concentration distribution of powders can be estimated reliably by means of ECT. The sensor is sufficiently short such that the material distribution within the length l of the sensing region is constant along axial direction. Hence, the cross-sectional average mass concentration can also be expressed by $\beta = m/V$, where m is the mass of the material within the sensor and $V = l\Gamma$ is the volume of the sensing region. In general the layer concentration is equal to the bulk density ρ_b, which can be expressed by $\rho_b = m/V_{mat}$ where $V_{mat} = l\Gamma_{mat}$ is the volume occupied by the material. Γ_{mat} is the cross-sectional area occupied by the material. With this the following relation is valid

$$\alpha = \frac{\Gamma_{mat}}{\Gamma} = \frac{l\Gamma_{mat}}{l\Gamma} = \frac{V_{mat}}{V} = \frac{\frac{m}{V}}{\frac{m}{V_{mat}}} = \frac{\beta}{\rho_b}. \tag{3}$$

Hence, the layer fraction α can be computed by the fraction of the cross-sectional average mass concentration β and the bulk density ρ_b of the powder.

For a circular cross-section of the pipe the relationship between the layer fraction α and the layer height h is given by [32]

$$\alpha = \frac{2 \arccos\left(1 - \frac{2h}{D}\right) - \sin\left(2 \arccos\left(1 - \frac{2h}{D}\right)\right)}{2\pi}. \tag{4}$$

The inverse of this relationship can be used to determine the layer height h from a layer fraction estimate.

To demonstrate the estimation of the layer height h from ECT-based signal evaluations material layers with defined heights are placed within the laboratory sensor. For this purpose a material holder is used to realize the material fillings within the sensor as it was also used in [30,48]. The material holder is made of 3D printed end caps and PET foil and fits exactly in the ECT sensor. The length of the material holder is 500 mm, which is significantly larger than the sensitive area of the ECT sensor (electrode length of 80 mm). Comparative simulation experiments revealed that the influence of the end caps is negligible and the capacitive measurements are comparable to those acquired for stationary layers between consecutive slugs. Fig. 7(a) depicts a comparison between the estimated layer heights h_{est} and the true layer heights h_{true} and Fig. 7(b) shows a sketch of the material holder used to perform the measurement experiments. An assessment of the estimated layer heights shows a good fit between the estimates and the true values of the layer height. The relative error is below 5 % over the whole measurement range. For $h/D > 0.3$ the error is in the scale of 1 %, which demonstrates the applicability of the proposed approach for the estimation of stationary layer heights by means of ECT.

3.4. Slug length

Another parameter, which is of interest for the study of flow mechanisms and also for the control of the flow process is the slug length L_s [11,49], since L_s directly influences the pressure drop along the conveying pipe [52].

The slug length can be determined from the slug velocity v_s and the duration of the slug core $T_s = T_2 - T_1$ by $L_s = T_s v_s$, where T_1 and T_2 are defined as depicted in Fig. 6. This relation holds if the change of the slug length over time, i.e. $\mathrm{d}L_s/\mathrm{d}t$ during the time interval in which the slug passes both sensor planes is negligible. This is the case when the slug front and the slug rear recorded by both sensor planes show the same time shift.

3.5. Slug velocity and particle velocity

The particle velocity v_p is the decisive velocity for the prediction of the pressure drop along the slug [32] as well as for the determination of the mass flow rate of the conveyed particles [53]. Since in horizontal slug flow processes with stationary layers the particle velocity v_p is in general lower than the slug velocity v_s a distinction between this velocities is crucial [11].

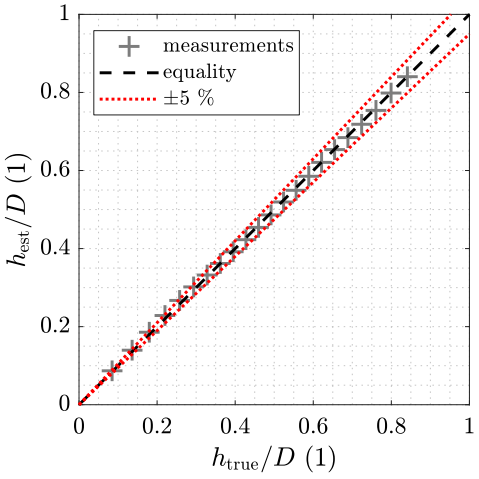

(a)

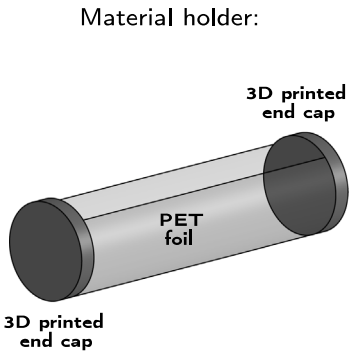

(b)

Fig. 7. (a) Comparison between the ECT-based layer height estimates and reference heights. (b) Material holder used to carry out measurement experiments with defined layer heights [30,48].

The slug velocity v_s can be determined from correlation analyses of multiple sensors, e.g. pressure signals [9,32] or dual-plane ECT sensors [16–18]. The particle velocity v_p can be determined from camera recordings of the flow and particle image velocimetry (PIV) analyses. PIV is the most common technique to obtain information about v_p [8,9]. PIV however has a limited applicability for the online determination of v_p especially in industrial environments. For this reason the determination of v_s as well as v_p by means of ECT is addressed in this subsection.

Fig. 8(a) depicts the cross-sectional average mass concentration β normalized by the bulk density ρ_b of the upstream and the downstream sensor for an exemplary slug flow experiment. The estimated signals show local signal variations within the slug signal trend, which originate from inhomogeneities in the material distribution within the slugs. These local signal variations are recorded by both sensor planes and they exhibit a larger time shift compared to the slug signal trend. For this reason it is hypothesized that the mass concentration signal is composed of the signal trend $\beta_0(t)$ caused by the slug, which is travelling at the slug velocity v_s and local signal variations $\Delta\beta(t)$ due to inhomogeneities within the slug, which are travelling at particle velocity v_p. Hence, the upstream sensor records the signal

$$\beta_{\text{upstr.}}(t) = \beta_0(t) + \Delta\beta(t), \tag{5}$$

and the downstream signal is given by

$$\beta_{\text{downstr.}}(t) = \beta_0(t + \Delta t_s) + \Delta\beta(t + \Delta t_p). \tag{6}$$

Hereby, $\Delta t_s = b/v_s$ and $\Delta t_p = b/v_p$ are the time shifts caused by the slug velocity and the particle velocity, respectively. b is the distance between the ECT sensors in m. To obtain $\Delta\beta(t)$ from the original signal $\beta(t)$ a ℓ_1 trend filter is applied to the signals [54–56]. With the trend filter, the signal trend can be estimated from the original signal by

$$\hat{\beta}_0 = \arg\min_{\beta_0} \sum_{j=1}^{n} \left(\beta_{0,j} - \beta_j\right)^2 + \lambda \sum_{j=1}^{n} \left|\nabla^2 \beta_{0,j}\right|, \tag{7}$$

where $\hat{\beta}_0$ denotes the estimate of the slug signal trend, n is the signal length, λ is a filter parameter and $\nabla^2\beta_{0,j} = \beta_{0,j} - 2\beta_{0,j-1} + \beta_{0,j-2}$ is the second order difference [54]. Given an estimate for the slug signal trend the local signal variations are obtained by $\Delta\hat{\beta} = \beta - \hat{\beta}_0$. Due to the steep signal gradients in the slug front and rear, the non-linear ℓ_1 trend filtering scheme outperforms linear filters like Savitzky–Golay filters [57], which are often proposed for trend filtering.

Fig. 8(a) also shows the estimated local signal variations within the slug signal trend based on the ℓ_1 filtering scheme for the marked time segments. Fig. 8(b) depicts the cross-correlation function for the original signals β as well as for the de-trended signals $\Delta\hat{\beta}$. The cross-correlation function of the de-trended signals shows the maximum at a larger time shift due to the fact that the particle velocity is smaller than the slug velocity. The time shifts between the signals correspond to a slug velocity of $v_s = 0.91\,\text{m}\,\text{s}^{-1}$ and a particle velocity of $v_p = 0.54\,\text{m}\,\text{s}^{-1}$. A PIV analysis of this experiment yields a average particle velocity within the slug of $v_p = 0.52\,\text{m}\,\text{s}^{-1}$, which indicates that the local inhomogeneities within a slug are travelling in fact with particle velocity.

Applying correlation analysis to the individual pixels of the cross-sectional estimates of the mass concentration distribution enables the estimation of velocity fields within the sensor [17,18,25]. Fig. 8(c) depicts a pixel-wise evaluation of the slug velocity and the particle velocity, which were obtained from the original signals and the de-trended signals of the pixels, respectively. The pixel-wise evaluation shows approximately constant slug velocities as well as particle velocities over the cross-section as it is also reported in several publications about horizontal slug flow pneumatic conveying [3,14,49].

Fig. 9(a) depicts a comparison between the PIV-based particle velocity and the ECT-based particle velocity for 51 slug flow experiments conducted on the laboratory test rig. The distribution of the error between the PIV-based particle velocities and the ECT-based particle velocities is shown in Fig. 9(b). The error distribution is approximately Gaussian with a mean of $\mu = -0.003\,\text{m}\,\text{s}^{-1}$ and a standard deviation of $\sigma = 0.012\,\text{m}\,\text{s}^{-1}$, which demonstrates the capability of ECT for the estimation of v_p. Note that the error distribution illustrates the fit between the ECT-based velocity estimates and the PIV measurements but cannot be interpreted as an uncertainty quantification of the ECT-based estimates as also the PIV measurements are subject to uncertainty [58]. Fig. 9(c) depicts the ECT-based slug velocity and particle velocity measurements for 51 flow experiments. On average, the relationship between v_s and v_p can be described by a straight line. Hereby, the slope of 0.86 corresponds to the average ECT-based slug to layer concentration ratio of $\bar{E}_{\text{ECT}} = 0.87$ as it is also reported in [5,9,11]. The constant part of $0.73\,\text{m}\,\text{s}^{-1}$ is slightly higher compared to results for plastic pellets presented in [9,11,19] where values in the range of

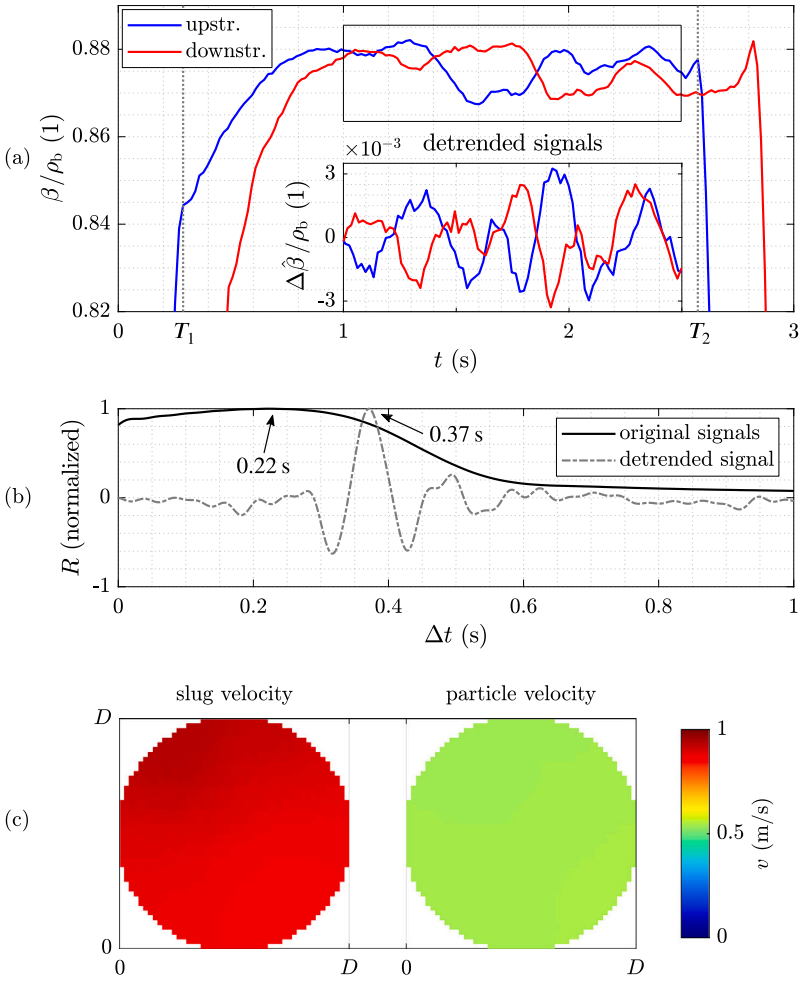

Fig. 8. (a) Upstream and downstream cross-sectional average mass concentration signals of a slug flow experiment on the laboratory test rig. The box shows the local signal variations within the slug signal trend for the marked time segment. (b) Cross-correlation function for the original signals and the de-trended signals. (c) Pixel-wise evaluation of the slug velocity and the particle velocity.

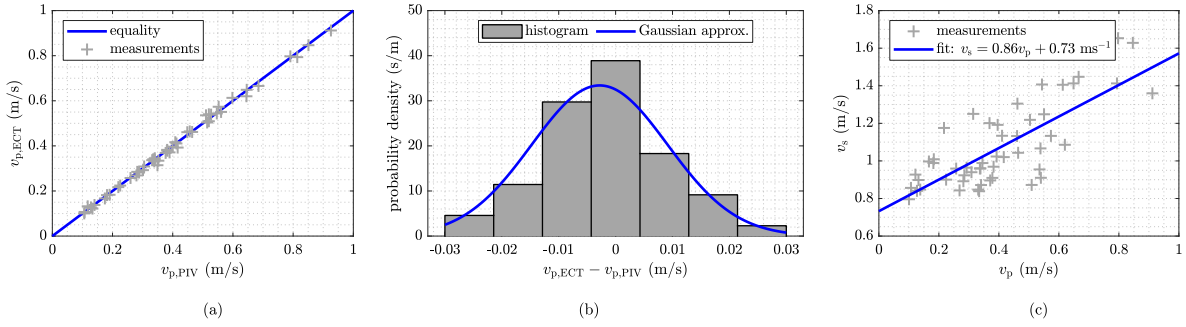

Fig. 9. ECT-based slug and particle velocity estimation. (a) Comparison between the ECT-based and the PIV-based particle velocity for 51 slug flow experiments in the laboratory test rig. (b) Distribution of the error between the ECT-based and the PIV-based particle velocity. (c) Relationship between the particle velocity and the slug velocity determined from ECT measurements.

$0.50\,\mathrm{m\,s^{-1}}$ to $0.67\,\mathrm{m\,s^{-1}}$ are reported. The increased constant originates from the increased pipe diameter of the flow test rig used in this work, which is in agreement with Konrad's gas–liquid analogy [59].

3.6. Additional reference material on ECT for flow parameter estimation

In Section 3 it was discussed how slug flow parameters can be estimated for ECT-based image reconstruction results. The estimation approaches are demonstrated on experiments conducted on the laboratory test rig depicted in Fig. 2. For detailed information about the implementation and the metrological properties of the algorithms we refer to the following literature [16,30,37,43].

4. Observations within an industrial process

In this section the application of the proposed ECT-based estimation techniques within an industrial scale pneumatic conveyor is presented.

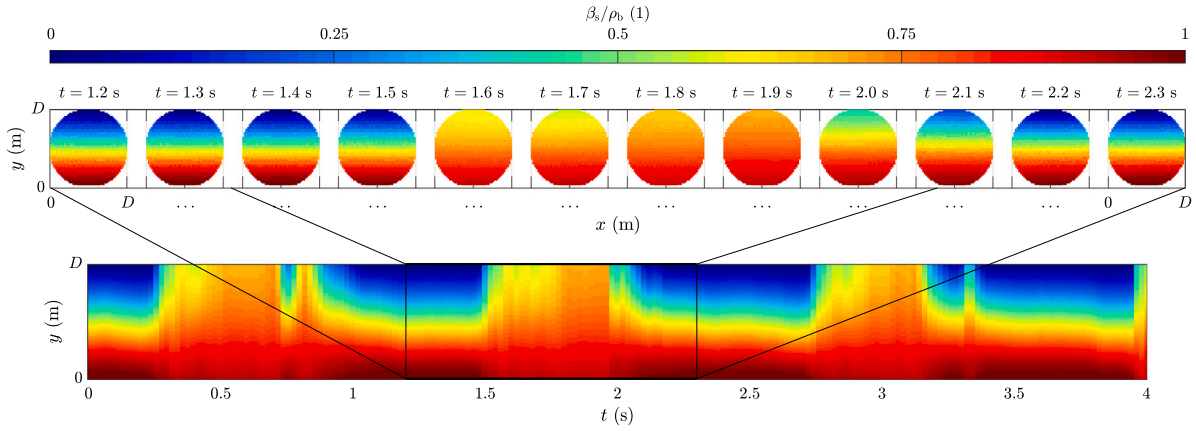

Fig. 10. Estimated mass concentration distribution within the industrial process plant showing multiple slugs separated by stationary layers. The transport good belongs to Geldart group A and has an Archimedes number of $Ar \approx$ 1e0.

4.1. General slug flow properties

4.1.1. Mass concentration distribution

Fig. 10 depicts the reconstructed mass concentration distribution of an exemplary data segment. The upper plot shows a series of cross-sectional mass concentration distributions $\beta(x, y)$. The lower plot depicts the time evolution of the height profile of the mass concentration within the conveying pipe $\beta(y, t)$.

The reconstructed mass concentration distribution shows a wave-like motion of the powder similar to the slug flow regime. Between the wave-like structures layers are observed at the bottom of the pipe, which reach the bulk density ρ_b of the powder. Due to this and the circumstance that the acquired measurement data of ECT system is uncorrelated within these layers it is concluded that these layers are stationary. Interestingly, slug-like structures with stationary layers are observed even though a Geldart group A powder with an Archimedes number of $Ar \approx$ 1e0 is conveyed. The flow regime chart presented in [3] states that slug flows with stationary layers only occurs for powders with $Ar >$ 1e2. Yet the tomographic data clearly shows a wave-like motion of the powder with stationary layers.

From $\beta(y, t)$ it can be seen, that the height of the layers separating the slugs decreases until the layer becomes stationary. This is attributed to the fluidization behaviour of Geldart group A powders. Geldart group A beds collapse slowly after de-fluidization, which is why it takes some time till the bed reaches the bulk density ρ_b of the powder [41]. For Geldart group D powders in contrast the layer is immediately stationary after the slug passes as it is shown in Fig. 6. The mass concentration within the slug is below the concentration of the layer and the mass concentration in the front of the slug core is lower compared to the centre of the slug core. This corresponds to observations of the laboratory experiments and to results reported in literature [11,32,51]. Hence, the mass concentration distribution in the process plant shows some similar properties compared to the slug flow of powders with $Ar >$ 1e2 [3,6]. Within the slug core however, the particles show a concentration gradient from the pipe bottom to the pipe top, i.e. the mass concentration at the bottom is slightly larger compared to the top of the pipe. This differs from the slug flow properties of powders with $Ar >$ 1e2 since they show homogeneous concentration distributions within the slug core as can be seen in Fig. 6.

4.1.2. Slug and particle velocity

Fig. 11 depicts the velocity field within the slug core. Similar to the result for Geldart group D powders depicted in Fig. 8(c) the slug velocity is approximately constant over the cross-section of the pipe and larger than the particle velocity. The particle velocity in contrast is inhomogeneous. Larger particle velocities occur at the top of the pipe and the particles at the pipe bottom are moving at a lower velocity. This

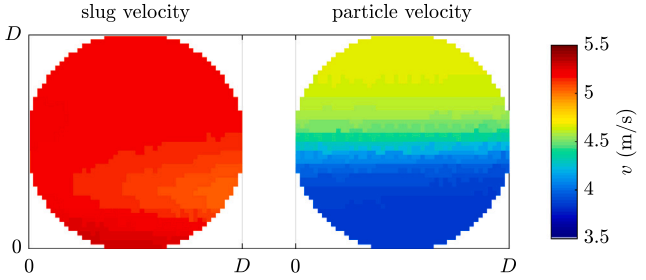

Fig. 11. Cross-sectional slug and particle velocity field of a slug flow process with a Geldart group A powder with $Ar \approx$ 1e0.

property is attributed to the mass concentration gradient within the slug core, i.e. particles are moving slower in regions with larger mass concentrations and vice versa. Slugs with non-homogeneous particle velocity fields within the slug core have been recently presented by [3] for $Ar >$ 1e2 described as small slugs moving at the top of a thick layer, which shows a velocity distribution along the y-axis. The flow process observed in this work in contrast seems to exhibit a significantly larger upper part with an increased particle velocity. The observed flow of pulverized coal clearly differs from the slug flow regime in a traditional sense as described in e.g. [6,11,32,59] and also from the slug flow regime of powders with $Ar >$ 1e2 and non-homogeneous particle velocity fields as described in [3]. Hence, the observed flow has to be distinguished from the slug flow regimes of powders with $Ar >$ 1e2, which are reported in literature.

Despite the differences between the observed dense phase flow and slug flow of powders with $Ar >$ 1e2, the flow regime is further referred to as slug flow and the wave-like structures as slugs.

4.1.3. Slug stability and steady state considerations

Fig. 12 depicts the measured layer fraction α as well as the measured slug length L_s of 712 consecutive slugs, which were conveyed over a duration of 15 min. Hereby, a threshold was applied to the measured signals in order to distinguish between slugs and layers. α and L_s are determined for consecutive slugs and layers ahead of the slug. The x-axis in Fig. 12 shows the discrete points in time where the slug front is recorded.

For a constant slug length the amount of material picked up from the stationary layer in front of the slug has to be the same than the amount of material deposited to the layer at the slug rear, i.e. the layer fraction at the front and the rear of the slug is the same [32]. Since the layer fraction α fluctuates strongly from one slug to another, unstable slugs with changing lengths are inferred. This corresponds to [15], where

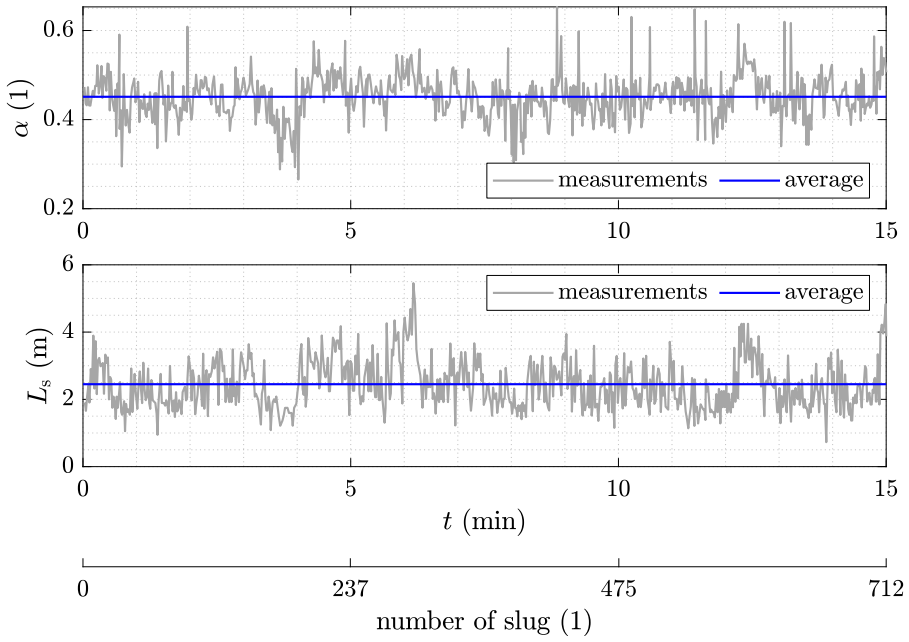

Fig. 12. Layer fraction and slug length measurements of consecutive slugs of a flow process with multiple slugs.

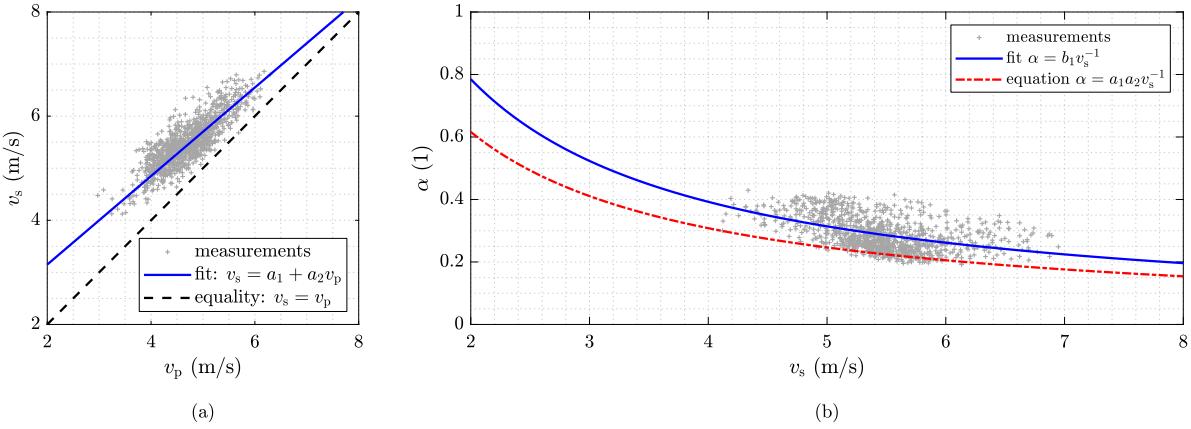

Fig. 13. Slug velocity, particle velocity and layer fraction measurements of a slug flow process with stationary layers.

it was concluded that individual slugs in an pneumatic conveyor of multiple slugs are unstable. However, the layer fraction α as well as the slug length L_s are fluctuating around constant average values indicating a overall steady state of the conveying process. This observation corresponds to the fact, that pneumatic conveyors operating in slug flow maintain a steady pressure drop even though parameters of individual slugs may vary in time [11].

4.1.4. Layer fraction and velocity relationship

Fig. 13(a) depicts slug and particle velocity measurements determined from ECT data, which was acquired over 24 h during a field experiment. Since the particle velocity was shown to be inhomogeneous within the slug core, cross-sectional average values are used. The velocity data shows that the average relationship between v_s and v_p can be described by a straight line $v_s = a_1 + a_2 v_p$. A least squares fit yields a constant part of $a_1 = 1.45\,\mathrm{m\,s^{-1}}$ and a slope of $a_2 = 0.85$. In [5] a model based on continuum mechanics is derived, which relates the slug velocity v_s and the particle velocity v_p. Hereby, a linear model of the form $v_s = E(v_p + c)$ was found, where E denotes the concentration ratio between the slug and the layer and c is the propagation velocity at which the particles travel relative to the slug. The derivation of this relationship is based on the assumption of homogeneous mass concentration distributions and particle velocity fields as it is the case for slug flow processes of powders with $Ar > 1e2$ [5–7,9,11,50]. The average concentration ratio of the shown data set obtained from ECT based mass concentration measurements is $\bar{E}_{ECT} = \beta_s/\rho_b = 0.82$. Interestingly, $\bar{E}_{ECT}$ fits well to the slope a_2 obtained from the least squares fit even though the observed flow regime shows non-homogeneous particle velocities and mass concentration distributions within the slugs. The constant part of $a_1 = 1.45\,\mathrm{m\,s^{-1}}$ however is significantly larger compared to results of powders with $Ar > 1e2$ reported in literature, which are in the range of $0.5\,\mathrm{m\,s^{-1}}$ to $0.67\,\mathrm{m\,s^{-1}}$ [9,19,32,59]. We attribute this deviation to the differing properties between the observed dense phase flow of pulverized coal and classical slug flows as described in e.g. [6,11,32,59]. Due to the slope being less than one a theoretical maximum particle velocity $v_{p,max} = a_1/(1 - a_2) = 9.67\,\mathrm{m\,s^{-1}}$ can be calculated [5]. At $v_{p,max}$ the particles start to outpace the slug, which should result in a transition away from the slug flow regime [9].

Fig. 13(b) depicts the relationship between the layer fraction α and the slug velocity v_s. A least squares fit of a function of the form $\alpha = b_1 v_s^{-1}$ shows that the layer fraction α is inversely proportional to the slug velocity v_s with $b_1 = 1.57\,\mathrm{m\,s^{-1}}$. For slug flow of powders with $Ar > 1e2$ the relationship between α and v_s was found to be $\alpha = E c v_s^{-1}$ [9,11].

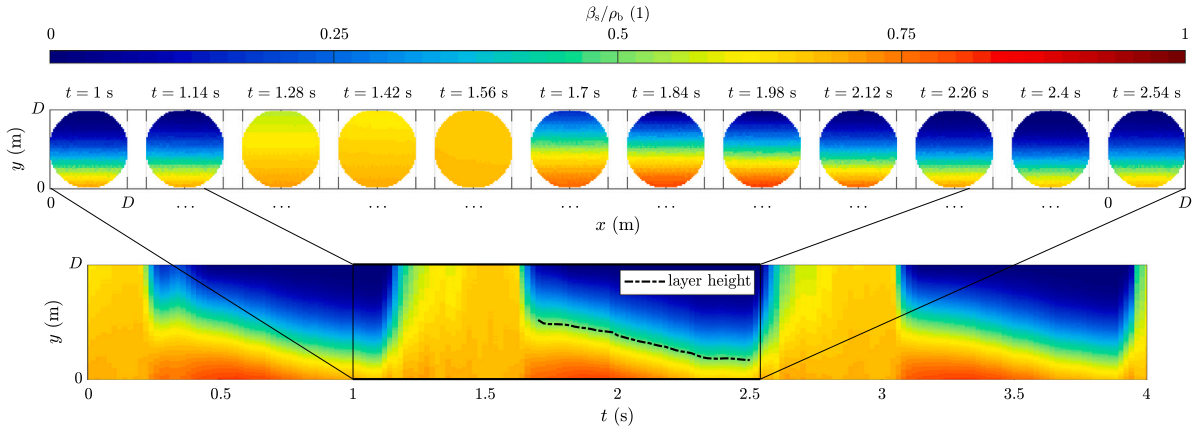

Fig. 14. Estimate mass concentration distribution of a flow process with a Geldart group A powder with $Ar \approx$ 1e0 showing multiple slugs separated by non-stationary layers.

This relation is again based on the assumption of homogeneous mass concentration distributions and particle velocity fields within the slug core as well as constant slug lengths, i.e. $\mathrm{d}L_s/\mathrm{d}t = 0$. Fig. 13(b) also shows the model $\alpha = Ec v_s^{-1}$ as it is described in [9]. Hereby, the values $c = a_1$ and $E = a_2$ are used, which are obtained from the least squares fit of the velocity data. Given the models described in [9] $a_1 a_2 = b_1$ should hold. For the data reported in this work however $a_1 a_2 = 1.23\,\mathrm{m\,s^{-1}}$ and $b_1 = 1.57\,\mathrm{m\,s^{-1}}$ is obtained. The values are in the same order of magnitude but differ from each other. Reasons for this deviation can be unstable individual slugs and inhomogeneous mass concentration distributions and non-constant particle velocity fields within the slug. Yet the measurements show an inversely proportional relationship between v_s and α as it is the case for slug flows of powders with $Ar >$ 1e2 [9,11,59].

4.2. Slugs with non-stationary layers

During the operation of the ECT system in the industrial process plant also slug flow with non-stationary layers is observed for Geldart group A powders with $Ar \approx$ 1e0. Slug flow with non-stationary layers was recently described in [3,32] for powders with $Ar >$ 1e2. In this subsection the ECT-based observations of slugs with non-stationary layers are discussed.

4.2.1. Mass concentration distribution

Fig. 14 depicts the estimated mass concentration distribution for an exemplary time segment in which the slug flow regime with moving layers is present. The upper plot shows a time series of cross-sectional mass concentration distributions $\beta(x, y)$ for a single slug and the layer behind the slug. The lower plot depicts the time evolution of the height profile of the mass concentration within the pipe $\beta(y, t)$ for multiple consecutive slugs. The reconstructed mass concentration distribution shows layers at the slug rear with a decreasing height over time indicating that the layer is not stationary but moving. The layer height h is indicated in the lower plot by the dashed line for an exemplary layer. This corresponds to the results for slugs with moving layers reported in [3,32]. In contrast to stationary layers the mass concentration of the moving layers is below the bulk density ρ_b. This is attributed to the movement of the material in the layers, which causes the layer to be fluidized to a certain extent so that the concentration of the bed does not reach ρ_b. Again the slug core shows a reduced mass concentration compared to the layer. The front of the slug core shows a lower mass concentration than the slug core, which is also comparable to slugs with stationary layers as depicted in Fig. 10 [11,32,51]. Compared to slugs with stationary layers the slug core exhibits a lower mass concentration.

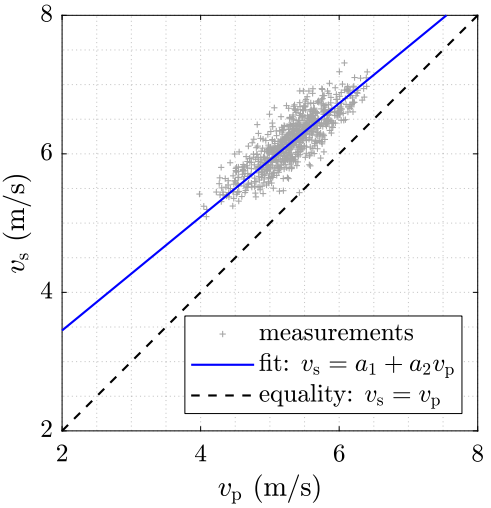

Fig. 15. Slug and particle velocity relationship for a slug flow process with non-stationary layers.

4.2.2. Slug and particle velocity relationship

Fig. 15 depicts ECT-based slug velocity v_s and particle velocity v_p measurements of slugs with non-stationary layers. The data was recorded during the same field experiment as the stationary layer data. The segmentation of the data into slug flow with stationary layers and slug flow with non-stationary layers is done based on the layer concentration β_l. Since $\beta_l \approx \rho_b$ for stationary layers and $\beta_l < \rho_b$ for non-stationary layers the data points for the individual flow regimes can be distinguished. A least squares fit shows again that the average relationship between v_s and v_p can be described by an affine function of the form $v_s = a_1 + a_2 v_p$. The least squares fit yields a constant part of $a_1 = 1.81\,\mathrm{m\,s^{-1}}$ and a slope of $a_2 = 0.82$. The slope fits again well to the average concentration ratio obtained from ECT-based mass concentration measurements, which is $\bar{E}_{\mathrm{ECT}} = 0.84$ for the data set shown in Fig. 15. The slug concentration as well as the layer concentration are reduced compared to stationary layer, which is why the concentration ratio E remains approximately constant. Again the constant part is significantly larger compared to results reported for powders with $Ar >$ 1e2 [9,19,32,59] and a_1 is also increased compared to the results presented for stationary layers. The increase of a_1 compared to slug flow with stationary layers however, coincides with the model described in [9] since the constant term increases by the layer velocity v_α in the case of non-stationary layers, i.e. $a_1 = c + v_\alpha$.

A comparison with the velocity data for stationary layers depicted in Fig. 13(a) shows that on average non-stationary layers occur at higher

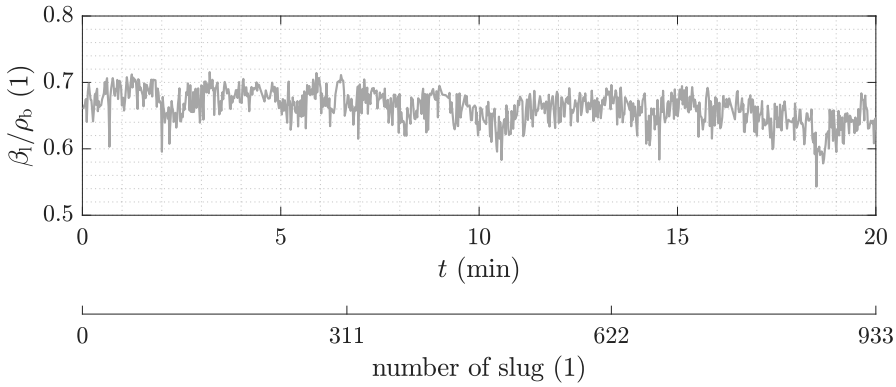

Fig. 16. Estimated layer concentration for an exemplary time segment of the field experiment where non-stationary layers are present for several consecutive slugs.

slug and particle velocities. However, the velocity ranges at which stationary and non-stationary layers occur are overlapping. Hence, the consideration of the velocities alone does not allow to draw conclusions about the stationarity of the layer indicating the existence of further influencing parameters.

4.2.3. Stability of the flow regime

In [9] it is reported, that slug flow with non-stationary layers is an intermediate flow regime, which occurs at a transition away from slug flow due to particles beginning to outpace the slug. However, observations based on ECT measurements revealed that in the case of pulverized coal with $Ar \approx 1e0$ non-stationary layers can be present for several minutes in which hundreds of consecutive slugs with non-stationary layers are sustained within the conveying pipe. Fig. 16 depicts the estimated layer concentration β_l for 933 consecutive slugs of an exemplary time segment of the field experiment with a duration of 20 min. The mass concentration of the layers is in the range of 60 % to 70 % of the bulk density ρ_b, which indicates that the layers are non-stationary over the whole duration of the shown time segment. Hence, even though non-stationary layers may be an indication that a further increase of the particle velocity lead to a transition away from the slug flow regime, it is a stable flow condition for the conveyed material.

4.3. Transition away from slug flow regime

Given the slug flow regime with non-stationary layers a further increase of the particle velocity results in an additional decrease of the mass concentration of the slug core and a change of the flow regime occurs. Fig. 17 depicts the estimated mass concentration distribution of a data segment with a duration of 200 s illustrating the transition away from the slug flow regime. The reconstruction result shows transitions from slugs to continuous flows e.g. at $t \approx 13$ s. The continuous flow segments exhibit dense bottom phases with a slowly varying height and a less dense top phase, which moves in a highly oscillating motion. This continuous material flow is sustained for up to approximately 15 s until slug like structures start to emerge again for several seconds, e.g. at $t \approx 45$ s. The flow condition is constantly changing between continuous material movement to slug like structures which are separated by layers making this transition flow regime highly unstable [60]. Interestingly the transitions are observed from particle velocities ranging from $v_p \approx 5.8\,\mathrm{m\,s^{-1}}$ to $v_p \approx 11\,\mathrm{m\,s^{-1}}$. Hence, the velocity range at which the transition occurs is overlapping with the velocity range at which the slug flow condition with non-stationary layers is present. The maximum particle velocity $v_{p,max} = 9.67\,\mathrm{m\,s^{-1}}$ predicted from the stationary layer data [9] is significantly larger than the minimum velocity at which the transitions occur. This indicates that for the conveyed material with $Ar \approx 1e0$ a consideration of the slug velocity and particle velocity alone is not sufficient for a prediction of a transition away from slug flow, which is why further influential parameters should be considered.

5. Conclusion

In this work the capabilities of ECT for flow parameter estimation in horizontal slug flow pneumatic conveying processes have been demonstrated. The estimation of crucial slug flow parameters based on tomographic signal evaluations are discussed. The estimation performance is demonstrated by means of laboratory experiments with Geldart group D powders with $Ar \approx 1e6$, for which reference data is available. It was shown that a dielectric characterization of powders enables the estimation of mass concentration distributions. In horizontal slug flow processes the velocity of the slug wave is in general larger compared to the velocities of the particles within the slug. It was demonstrated, that information about the particle velocity can be obtained from local signal variations within the slug signal trend of the estimated mass concentration signals. Hereby a signal de-trending scheme is applied to enable cross-correlation analyses of the local signal variations recorded by a dual-plane ECT system, which yields the particle velocity field within the slug core. The potential of ECT to estimate mass concentration distributions as well as the velocity of the particles gives access to future developments of ECT-based mass flow meters for horizontal slug flow processes.

The proposed estimation techniques have been applied to data provided by an ECT system, which is installed within a large scale pneumatic conveyor of an industrial process plant. Hereby, various consistencies with results reported in available literature are shown but also novel insights into horizontal slug flow processes of multiple slugs could be obtained. It was observed that in contrast to available literature also Geldart group A powder with Archimedes numbers in the scale of $Ar \approx 1e0$ can be conveyed in slug-like structures which are separated by stationary layers. For the observed dense phase flow of pulverized coal various similarities between the slug flow regime of powders with $Ar > 1e2$ could be confirmed but also deviating properties were observed, i.e. non-homogeneous mass concentration distributions and non-constant particle velocity fields within the slug core. For increased particle velocities non-stationary layers occurred. Even though slug flow with non-stationary layers forms an intermediate flow condition between slug flow with stationary layers and a transition away from slug flow it was observed that slug flow with non-stationary layers can be sustained for several minutes in which hundreds of consecutive slugs are conveyed. For a further increase of the particle velocity a transition away from slug flow was observed. Hereby, a continuous particle flow occurs for several seconds until slug like structures emerge again. The flow is constantly changing from continuous material movement to slug like structures making this transition flow regime unstable. Additionally, it was observed that the transition away from slug flow starts to occur at particle velocities significantly below the theoretical maximum particle velocity predicted from slug velocity and particle velocity data, indicating further dependencies of the flow regime with other parameters.

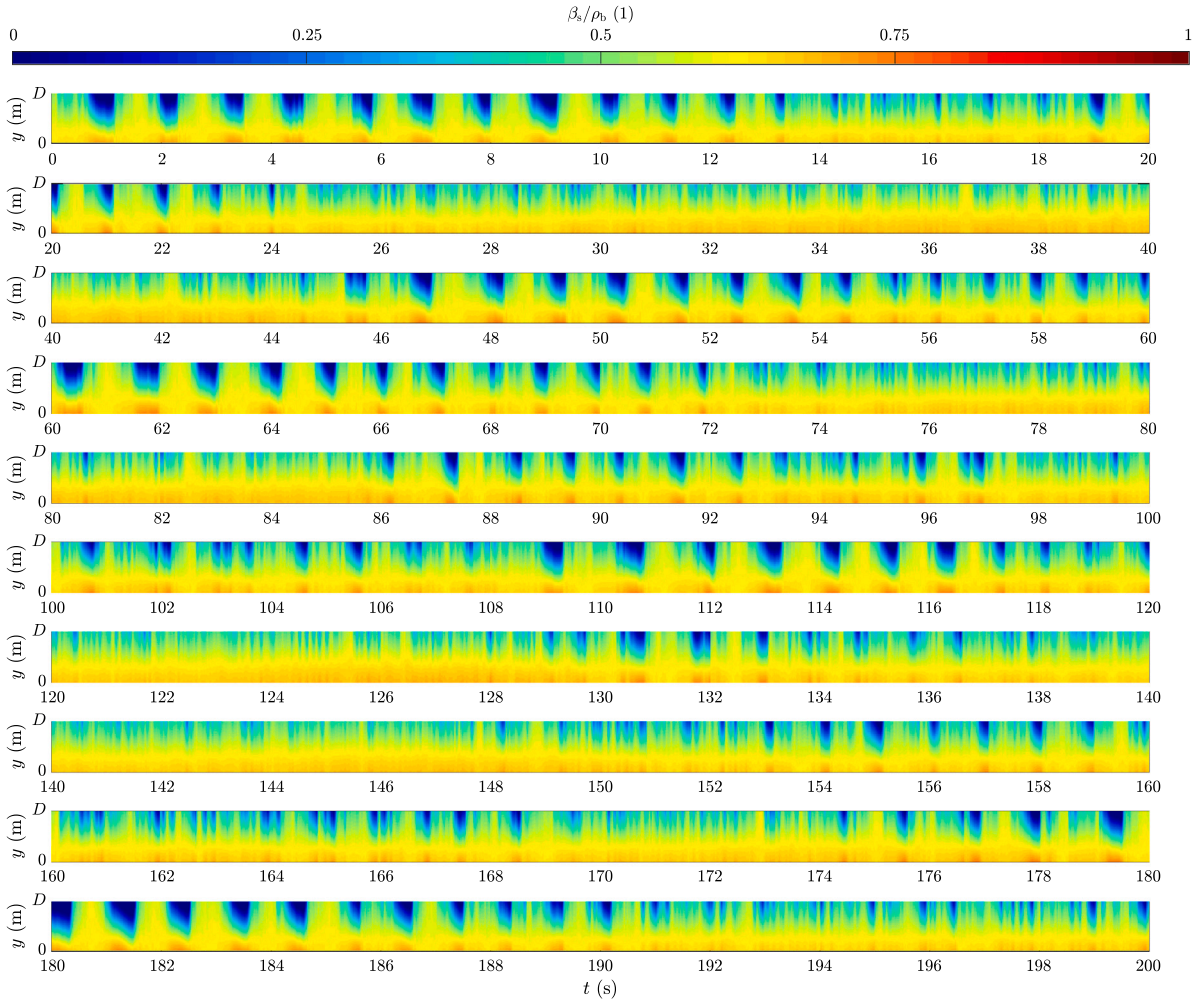

Fig. 17. Mass concentration distribution of an unstable flow conditions, which occurs at a transition away from slug flow.

In conclusion, the results presented in this work are pointing out the capabilities of ECT to analyse complex and highly dynamical dense phase flow processes. The techniques presented in this work enable the development of potential flow meters for horizontal slug flow processes, which are crucial for process control and a reliable operation of dense phase conveying processes. Furthermore, the proposed estimation techniques give access to further insights and a deeper understanding of the flow mechanisms involved in horizontal slug flow processes.

CRediT authorship contribution statement

Thomas Suppan: Conceptualization, Methodology, Software, Investigation, Writing – original draft. **Markus Neumayer:** Conceptualization, Methodology, Writing – review & editing, Supervision. **Thomas Bretterklieber:** Conceptualization, Writing – review & editing, Supervision. **Stefan Puttinger:** Conceptualization, Writing – review & editing. **Christoph Feilmayr:** Conceptualization, Writing – review & editing. **Stefan Schuster:** Conceptualization, Writing – review & editing. **Hannes Wegleiter:** Conceptualization, Writing – review & editing, Project administration, Funding acquisition.

Declaration of competing interest

The authors declare that they have no known competing financial interests or personal relationships that could have appeared to influence the work reported in this paper.

Data availability

The data that has been used is confidential.

Acknowledgements

The financial support by the Austrian Federal Ministry for Digital and Economic Affairs, the National Foundation for Research, Technology and Development and the Christian Doppler Research Association is gratefully acknowledged.

References

[1] G.E. Klinzing, A review of pneumatic conveying status, advances and projections, Powder Technol. 333 (2018) 78–90.
[2] G.E. Klinzing, Historical review of pneumatic conveying, KONA Powder Part. J. 35 (2018) 150–159.
[3] H. Kalman, A. Rawat, Flow regime chart for pneumatic conveying, Chem. Eng. Sci. 211 (2020) 115256.
[4] K. Konrad, Dense-phase pneumatic conveying: A review, Powder Technol. 49 (1) (1986) 1–35.
[5] O. Orozovic, A. Lavrinec, F. Georgiou, C. Wensrich, A continuum mechanics derivation of the empirical expression relating slug and particle velocities, Powder Technol. 380 (2021) 598–601.
[6] S. Shaul, H. Kalman, Three plugs model, Powder Technol. 283 (2015) 579–592.
[7] S. Shaul, H. Kalman, Investigating the conveying mechanism of particulate plugs with stationary layers, Powder Technol. 272 (2015) 322–331.
[8] A. Lavrinec, O. Orozovic, H. Rajabnia, K. Williams, M.G. Jones, G. Klinzing, Inertial measurement unit as a tool within dense phase pneumatic conveying. Investigation into velocity measurement accuracy, pressure and velocity relationships in slug flow, Powder Technol. 382 (2021) 454–466.

[9] O. Orozovic, A. Lavrinec, Y. Alkassar, J. Chen, K. Williams, M.G. Jones, G.E. Klinzing, Insights into horizontal slug flow pneumatic conveying from layer fraction and slug velocity measurements, Powder Technol. 364 (2020) 218–228.

[10] O. Orozovic, A. Lavrinec, H. Rajabnia, K. Williams, M.G. Jones, G.E. Klinzing, Transport boundaries and prediction of the slug velocity and layer fraction in horizontal slug flow pneumatic conveying, Chem. Eng. Sci. 227 (2020) 115916.

[11] O. Orozovic, A. Lavrinec, Y. Alkassar, K. Williams, M.G. Jones, G. Klinzing, On the kinematics of horizontal slug flow pneumatic conveying and the relationship between slug length, porosity, velocities and stationary layers, Powder Technol. 351 (2019) 84–91.

[12] J. Zhou, L. Shangguan, K. Gao, Y. Wang, Y. Hao, Numerical study of slug characteristics for coarse particle dense phase pneumatic conveying, Powder Technol. 251 (2021) 15–24.

[13] K. Li, S.B. Kuang, R.H. Pan, A.B. Yu, Numerical study of horizontal pneumatic conveying: Effect of material properties, Powder Technol. 251 (2014) 15–24.

[14] R.E. Stratton, C.M. Wensrich, Horizontal slug flow pneumatic conveying: Numerical simulation and analysis of a thin slice approximation, Powder Technol. 214 (2011) 477–490.

[15] O. Orozovic, H. Rajabnia, A. Lavrinec, M.H. Meylan, K. Williams, M.G. Jones, G.E. Klinzing, Individual slugs in a pneumatic conveyor of multiple slugs are likely unstable, Chem. Eng. Sci. 250 (2022) 117365.

[16] T. Suppan, M. Neumayer, T. Bretterklieber, S. Puttinger, C. Feilmayr, H. Wegleiter, ECT-based mass flow metering in pneumatic conveying processes, in: Proceedings of the 10th World Congress on Industrial Process Tomography, 2021.

[17] V. Mosorov, G. Rybak, D. Sankowski, Plug regime flow velocity measurement problem based on correlability notion and twin plane electrical capacitance tomography: Use case, Sensors 21 (6) (2021) 2189.

[18] C.O. Maung, D. Kawashima, H. Oshima, Y. Tanaka, Y. Yamane, M. Takei, Particle volume flow rate measurement by combination of dual electrical capacitance tomography sensor and plug flow shape model, Powder Technol. 364 (2020) 310–320.

[19] C. Nied, J.A. Lindner, K. Sommer, On the influence of the wall friction coefficient on void fraction gradients in horizontal pneumatic plug conveying measured by electrical capacitance tomography, Powder Technol. 321 (2017) 310–317.

[20] M. Neumayer, G. Steiner, D. Watzenig, Electrical capacitance tomography: Current sensors/algorithms and future advances, in: 2012 IEEE International Instrumentation and Measurement Technology Conference Proceedings, 2012, pp. 929–934.

[21] M. Neumayer, H. Zangl, D. Watzenig, A. Fuchs, Developments and applications in sensing technology, in: S.C. Mukhopadhyay, A. Lay-Ekuakille, A. Fuchs (Eds.), New Developments and Applications in Sensing Technology, Springer Berlin Heidelberg, Berlin, Heidelberg, 2011, pp. 65–106.

[22] W. Yang, Design of electrical capacitance tomography sensors, Meas. Sci. Technol. 21 (4) (2010) 042001.

[23] T. Suppan, M. Neumayer, T. Bretterklieber, H. Wegleiter, S. Puttinger, Measurement methodology to characterize permittivity-mass concentration relations of aerated bulk materials, in: 2021 IEEE International Instrumentation and Measurement Technology Conference, I2MTC, 2021, pp. 1–6.

[24] M. Neumayer, M. Flatscher, T. Bretterklieber, Coaxial probe for dielectric measurements of aerated pulverized materials, IEEE Trans. Instrum. Meas. 68 (5) (2019) 1402–1411.

[25] U. Datta, T. Dyakowski, S. Mylvaganam, Estimation of particulate velocity components in pneumatic transport using pixel based correlation with dual plane ECT, Chem. Eng. J. 130 (2) (2007) 87–99.

[26] R.K. Rasel, S.M. Chowdhury, Q.M. Marashdeh, F.L. Teixeira, Review of selected advances in electrical capacitance volume tomography for multiphase flow monitoring, Energies 15 (14) (2022).

[27] D. Wang, M. Xu, Q. Marashdeh, B. Straiton, A. Tong, L.-S. Fan, Electrical capacitance volume tomography for characterization of gas-solid slugging fluidization with geldart group d particles under high temperatures, Ind. Eng. Chem. Res. 57 (2018).

[28] A. Wang, Q. Marashdeh, B.J. Motil, L.-S. Fan, Electrical capacitance volume tomography for imaging of pulsating flows in a trickle bed, Chem. Eng. Sci. 119 (2014) 77–87.

[29] W. Thielicke, E.J. Stamhuis, PIVlab – towards user-friendly, affordable and accurate digital particle image velocimetry in MATLAB, J. Open Res. Softw. 2 (2014).

[30] T. Suppan, M. Neumayer, T. Bretterklieber, S. Puttinger, H. Wegleiter, A model-based analysis of capacitive flow metering for pneumatic conveying systems: A comparison between calibration-based and tomographic approaches, Sensors 22 (2022) 856.

[31] M. Sun, S. Liu, J. Lei, Z. Li, Mass flow measurement of pneumatically conveyed solids using electrical capacitance tomography, Meas. Sci. Technol. 19 (4) (2008) 045503.

[32] A. Rawat, H. Kalman, Particle velocity and stationary layer height analysis for modification and validation of particulate plug-2 pressure drop model, Powder Technol. 361 (2020) 867–879.

[33] X. Cong, X. Guo, H. Lu, X. Gong, K. Liu, X. Sun, K. Xie, Flow patterns of pulverized coal pneumatic conveying and time-series analysis of pressure fluctuations, Chem. Eng. Sci. 101 (2013) 303–314.

[34] X. Cong, X. Guo, X. Gong, H. Lu, K. Liu, H. Qi, Investigations of pulverized coal pneumatic conveying using CO2 and air, Powder Technol. 219 (2012) 135–142.

[35] X. Cong, X. Guo, X. Gong, H. Lu, W. Dong, Experimental research of flow patterns and pressure signals in horizontal dense phase pneumatic conveying of pulverized coal, Powder Technol. 208 (3) (2011) 600–609.

[36] B. Azzopardi, K. Jackson, J. Robinson, R. Kaji, M. Byars, A. Hunt, Fluctuations in dense phase pneumatic conveying of pulverised coal measured using electrical capacitance tomography, Chem. Eng. Sci. 63 (9) (2008) 2548–2558.

[37] T. Suppan, M. Neumayer, T. Bretterklieber, H. Wegleiter, Thermal drifts of capacitive flow meters: Analysis of effects and model-based compensation, IEEE Trans. Instrum. Meas. 70 (2021) 1–11.

[38] M. Flatscher, M. Neumayer, T. Bretterklieber, Holistic analysis for electrical capacitance tomography front-end electronics, J. Phys. Conf. Ser. 1065 (2018) 092008.

[39] Z. Cui, H. Wang, Z. Chen, Y. Xu, W. Yang, A high-performance digital system for electrical capacitance tomography, Meas. Sci. Technol. 22 (5) (2011) 055503.

[40] H. Wegleiter, A. Fuchs, G. Holler, B. Kortschak, Development of a displacement current-based sensor for electrical capacitance tomography applications, Flow Meas. Instrum. 19 (5) (2008) 241–250.

[41] D. Geldart, Types of gas fluidization, Powder Technol. 7 (5) (1973) 285–292.

[42] S. Matsusaka, H. Maruyama, T. Matsuyama, M. Ghadiri, Triboelectric charging of powders: A review, Chem. Eng. Sci. 65 (2010) 5781–5807.

[43] T. Suppan, M. Neumayer, T. Bretterklieber, S. Puttinger, Prior design for tomographic volume fraction estimation in pneumatic conveying systems from capacitive data, Trans. Inst. Meas. Control 42 (4) (2020) 716–728.

[44] T. Suppan, M. Neumayer, T. Bretterklieber, S. Puttinger, Volume fraction estimation in pneumatic conveying from tomographic measurements, in: Proceedings of the 9th World Congress on Industrial Process Tomography, Vol. 3, 2018, pp. 667–675.

[45] M. Neumayer, T. Bretterklieber, M. Flatscher, S. Puttinger, PCA based state reduction for inverse problems using prior information, COMPEL - Int. J. Comput. Math. Electr. Electron. Eng. 36 (5) (2017) 1430–1441.

[46] D. Dube, Study of Landau-Lifshitz-Looyenga's formula for dielectric correlation between powder and bulk, J. Phys. D: Appl. Phys. 3 (11) (1970) 1648–1652.

[47] H. Looyenga, Dielectric constants of heterogeneous mixtures, Physica 31 (3) (1965) 401–406.

[48] T. Suppan, M. Neumayer, T. Bretterklieber, H. Wegleiter, S. Puttinger, Performance assessment framework for electrical capacitance tomography based mass concentration estimation in pneumatic conveying systems, in: 2021 IEEE International Instrumentation and Measurement Technology Conference, I2MTC, 2021, pp. 1–6.

[49] O. Orozovic, H. Rajabnia, A. Lavrinec, M.H. Meylan, K. Williams, M.G. Jones, G.E. Klinzing, An inequality relating fundamental parameters of horizontal slug flow pneumatic conveying, Chem. Eng. Res. Des. 177 (2022) 759–766.

[50] A. Lavrinec, O. Orozovic, K. Williams, M.G. Jones, G. Klinzing, W. Clark, Z. Wang, Observations of dense phase pneumatic conveying using an inertial measurement unit, Powder Technol. 343 (2019) 436–444.

[51] S.B. Kuang, K.W. Chu, A.B. Yu, Z.S. Zou, Y.Q. Feng, Computational investigation of horizontal slug flow in pneumatic conveying, Ind. Eng. Chem. Res. 47 (2008) 470–480.

[52] I. Lecreps, O. Orozovic, M.G. Jones, K. Sommer, Application of the principles of gas permeability and stochastic particle agitation to predict the pressure loss in slug flow pneumatic conveying systems, Powder Technol. 254 (2014) 508–516.

[53] Y. Yan, D. Stewart, Guide to the Flow measurement of Particulate Solids in Pipelines, Institute of Measurement and Control, National Engineering Laboratory and the University of Greenwich, 2001.

[54] A.K. Roonizi, ℓ_2 And ℓ_1 trend filtering: A Kalman filter approach [lecture notes], IEEE Signal Process. Mag. 38 (6) (2021) 137–145.

[55] S.-J. Kim, K. Koh, S. Boyd, D. Gorinevsky, ℓ_1 Trend filtering, SIAM Rev. 51 (2) (2009) 339–360.

[56] S.-J. Kim, K. Koh, M. Lustig, S. Boyd, D. Gorinevsky, An interior-point method for large-scale ℓ_1-regularized least squares, IEEE J. Sel. Top. Sign. Proces. 1 (4) (2007) 606–617.

[57] R.W. Schafer, What is a Savitzky-Golay filter? [lecture notes], IEEE Signal Process. Mag. 28 (4) (2011) 111–117.

[58] A. Sciacchitano, Uncertainty quantification in particle image velocimetry, Meas. Sci. Technol. 30 (9) (2019) 092001.

[59] K. Konrad, J. Davidson, The gas—liquid analogy in horizontal dense-phase pneumatic conveying, Powder Technol. 39 (2) (1984) 191–198.

[60] G. Jama, G. Klinzing, F. Rizk, An investigation of the prevailing flow patterns and pressure fluctuation near the pressure minimum and unstable conveying zone of pneumatic transport systems, Powder Technol. 112 (2000) 87–93.